Geophysical Research Letters

RESEARCH LETTER
10.1029/2023GL105427

Key Points:

- Anthropogenic aerosol removal will accelerate the Tibetan Plateau (TP) warming induced by greenhouse gas emission over the coming decades
- The TP will warm by 1.85°C (2.69°C) in 2041–2060 (2081–2100) relative to 1995–2014 under intermediate-emission scenario
- Constrained responses to individual external forcings projects weaker TP warming than the raw projections

Supporting Information:

Supporting Information may be found in the online version of this article.

Correspondence to:

T. Zhou,
zhoutj@lasg.iap.ac.cn

Citation:

Jiang, J., & Zhou, T. (2023). Observational constraint on the contributions of greenhouse gas emission and anthropogenic aerosol removal to Tibetan Plateau future warming. *Geophysical Research Letters*, *50*, e2023GL105427. https://doi.org/10.1029/2023GL105427

Received 17 JUL 2023
Accepted 22 AUG 2023

Observational Constraint on the Contributions of Greenhouse Gas Emission and Anthropogenic Aerosol Removal to Tibetan Plateau Future Warming

Jie Jiang[1] and Tianjun Zhou[1,2]

[1]State Key Laboratory of Numerical Modeling for Atmospheric Sciences and Geophysical Fluid Dynamics, Institute of Atmospheric Physics, Chinese Academy of Sciences, Beijing, China, [2]University of the Chinese Academy of Sciences, Beijing, China

Abstract A decline of anthropogenic aerosol (AA) emission is expected worldwide over the coming decades. But the climate effects of aerosol removal and greenhouse gases (GHG) emission at regional scale are poorly distinguished and constrained. Taking the Tibetan Plateau (TP) as an instance, analyses of the state-of-the-art climate models participating in the Detection and Attribution Model Intercomparison Project imply that while the observed warming from 1961 to 2020 is predominantly attributed to GHG emission, the future temperature rise will be influenced by the combined effects of persistent increase in GHG concentration and reduction of AA emission. Here, we develop a new constraint method considering the changed contribution of AA forcing. Constrained by detected individual external forcings, the joint contributions of GHG (1.74°C) and AA forcings (0.10°C) will lead to a warming around 1.85°C over the TP during mid-century (2041–2060) relative to 1995–2014 under SSP2-4.5 scenario, which is 0.44°C cooler than the raw projection.

Plain Language Summary The rapid warming over the Tibetan Plateau (TP) has led to increased risks to ecological environment and even the livelihoods and health of the people. A reliable projection on future warming and a deeper understanding of the contributions of the effects of anthropogenic aerosol (AA) removal and greenhouse gases (GHG) emission are necessary for climate change adaptation and mitigation activities. Here, using the state-of-the-art climate models participating in the Detection and Attribution Model Intercomparison Project, we found that the while the GHG emission has and will continue to warm the TP from 1961 to 2100, the changes in AA emission have partly offset the warming trend induced by GHG forcing before the late 2000s but will accelerate the warming rate induced by GHG forcing in the future. According to on our new constraint method considering the changed emission condition of AA, the joint contributions of GHG emission (1.74°C) and AA removal (0.10°C) will lead to a warming around 1.85°C over the TP during mid-century (2041–2060) relative to 1995–2014 under intermediate-emission scenario. Both the effects of GHG and AA to TP future warming are overestimated by the state-of-the-art climate models.

1. Introduction

The Tibetan Plateau (hereafter TP) is widely known as the "Third Pole" or "Asian Water Tower," and provides crucial water resources to nearly one fifth of the world's population (Immerzeel & Bierkens, 2012; X. Xu et al., 2008; Yao et al., 2022). The TP is an ecologically fragile area and is highly sensitive to climate changes (Immerzeel et al., 2010). Since the early 1950s, a rapid warming is observed over this extremely cold region, which is nearly twice the synchronous global mean (Duan & Xiao, 2015; X. Liu et al., 2009; Yao et al., 2019), resulting in serious ecological and environment problems (Azam et al., 2018; Bolch et al., 2012; Cuo et al., 2020; M. Yang et al., 2010; Yao et al., 2022). The amplified warming over the TP is related with snow/ice-albedo feedback, cloud-radiation interaction, water vapor feedback and underlying surface changes (You et al., 2020, 2021a). Understanding the observed TP warming is crucial for climate change adaptation and mitigation activities in this ecologically fragile area.

Both the internal variability and external forcings can modulate the long-term changes in surface air temperature (SAT) over the TP. For example, the warm phase of Atlantic Multidecadal Oscillation is favorable for a warmer condition over the TP, and vice versa, which is related with the mid-latitude westerly anomalies (Shi et al., 2017; J. Wang et al., 2013, 2014). The Pacific Decadal Oscillation can also modulate TP SAT at interdecadal time scale as supported by the temperature reconstructions (Yin et al., 2021; Y. Zhang et al., 2021).

In terms of external forcings, a detection and attribution study based on global climate models participating Coupled Model Intercomparison Project Phase 5 (CMIP5) showed that the observed TP warming during 1961–2005 is attributable to human influences, especially the continued emission of greenhouse gases (GHG) (Zhou & Zhang, 2021), which is mainly caused by the thermodynamic processes related to radiative forcing (Y. Wang et al., 2023).

Given the evidence that the rapid warming over the TP could lead to increased risks to ecological environment and even the livelihoods and health of the people, a reliable projection on the future changes of SAT over this region is necessary. Both the earlier generation of climate models from CMIP5 and the state-of-the-art climate models provided by CMIP6 (Coupled Model Inter-comparison Project- phase 6) suggest that there is a continued warming over the TP in the twenty-first century under different scenarios (Chen et al., 2022; Zhou & Zhang, 2021). As the two generation of climate models produce strong cold biases over most parts of the TP in past decades (Chen et al., 2022; Peng et al., 2022; Zhou & Zhang, 2021), recent studies worried that the biases in climate models in reproducing the observational historical trends and the large spread of the future projection among the models may reduce the credibility of the existing projections (X. Yang et al., 2021; You et al., 2021b; Zhu & Yang, 2020). Multiple methods had been proposed to constrain the projected SAT changes, for example, using weights considering model skill and independence for the ensemble mean (Liang et al., 2020), applying the attribution results of historical trends to projections (Ribes et al., 2021; Stott et al., 2006), or establishing the relationship between the simulated historical warming trend in recent decades and future changes (Tokarska et al., 2020).

The attribution results of historical trends are widely used to constrain future climate projection at regional scale. Previous studies on future projections usually scaled the projected response to the combined external forcings by the regression coefficient derived from the regression analysis in the historical period by using the fingerprinting technique (Allen et al., 2000; Sun et al., 2014; Zhou & Zhang, 2021). However, since the anthropogenic aerosols (AA) are expected to decrease while the GHG would continue to increase in the future scenarios, the compound impact of GHG and AA in historical changes measured by the regression coefficient derived from the fingerprinting method may not work in the future. Hence it is necessary to distinguish the impact of individual external forcings. The Detection and Attribution Model Intercomparison Project (DAMIP) of CMIP6 not only provides individual-forcing simulations in the past but also provides individual-forcing projections under SSP2-4.5 scenario (Gillett et al., 2016). In this study, we first attribute the observed TP warming from 1961 to 2020 using the newly available CMIP6 data. We then constrain the projection by the detected observational responses to individual external forcings and quantified the contributions of greenhouse gas emission and anthropogenic aerosol removal to TP future warming. This information is crucial for social planning to the public and policymakers.

2. Data and Methods

2.1. Observed Data

To show how warm the TP is in the recent six decades, three sets of gridded SAT data sets are used: (a) the SAT data sets provided by the National Meteorological Information Center of China (CN05.1) with a spatial resolution of $0.25° \times 0.25°$ (Wu & Gao, 2013; Y. Xu et al., 2009); (b) the Berkeley Earth Surface Temperatures (BEST) with a spatial resolution of $1° \times 1°$ (Rohde & Hausfather, 2020); and (c) the SAT data set constructed by the Climatic Research Unit (CRU) with a spatial resolution of $0.5° \times 0.5°$ (Harris et al., 2014). The detailed information can be found in Table S1 of the Supporting Information S1. Since the CN05.1 data set is based on stations operated by China Meteorological Administration and only covers the major parts of the plateau, all data sets are first interpolated onto the same spatial resolution of $1° \times 1°$ by using the bilinear interpolation method and then masked as in CN05.1 to facilitate comparison.

Observation records from meteorological stations are also used to evaluate the applicability of the gridded SAT data sets over the TP. Daily SAT collected by the China Meteorological Administration at 93 meteorological stations in the TP from 1961 to 2020 with rigorous quality control procedures is used (Cao et al., 2016). The year (month) with more than 1 month (3 days) of missing data is excluded. And only stations with records of more than 57 years (95%) are used to calculate the warming rates. Station observation is transformed into gridded data set with the same spatial resolution of $1° \times 1°$. As the stations are sparsely distributed over the TP (Figure S1a in Supporting Information S1), to reduce the uncertainty from interpolation, SAT at stations falling within a grid cell is averaged as the observed SAT of that grid cell (Figure S1b in Supporting Information S1).

2.2. CMIP6 Model Simulations

We use 12 CMIP6 models in our detection and attribution analysis and this is the largest amounts of models that provide the essential data. These models are selected as they provide historical simulations, hist-nat simulations, hist-GHG simulations, hist-aer simulations and SSP2-4.5 projections and have more than one realization for historical simulations and SSP2-4.5 projections (Table S2 in Supporting Information S1). The historical simulations covering the period of 1850–2014 are forced by both natural and anthropogenic external forcings. The hist-nat, hist-GHG and hist-aer simulations covering the period of 1850–2020 are forced by natural variability, GHG, or anthropogenic aerosols alone, respectively, and are referred as NAT, GHG, and AA. The historical simulations were extended to 2020 following the SSP2-4.5 emission scenario and are referred as ALL. A common study period of 1961–2020 as in observations are used. The piControl simulations of the 12 CMIP6 models are also used to estimate the internal variability. All simulations are interpolated onto the same spatial resolution of CN05.1 by using the bilinear interpolation method and then masked as in CN05.1.

Climate projections driven by a set of emissions and land use scenarios based on socioeconomic, environmental and technological trends are effective tools for climate impact, mitigation and adaptation studies (O'Neill et al., 2016; Rao et al., 2017). DAMIP provides individual-forcing projections under SSP2-4.5 scenario to understand the impact of different external forcings in the future. This scenario was chosen as it combines the intermediate forcing level and the intermediate societal vulnerability, and can represent a broad range of Shared Socioeconomic Pathway-based integrated assessment model projections (Gillett et al., 2016; O'Neill et al., 2016). Among the 12 CMIP6 models used for detection and attribution, CanESM5, GISS-E2-1-G, MIROC6 and NorESM2-LM have uploaded projections under GHG, AA and NAT forcings, and are referred as *M4*.

2.3. Methods

The optimal fingerprinting method is employed for detection and attribution (Allen & Stott, 2003; Allen & Tett, 1999; Hasselmann, 1993; Hegerl & Zwiers, 2011). The method is based on a total least square regression model and can be expressed as $y = \sum_{i=1}^{m} \beta_i \left(X_i - \varepsilon_{x_i}\right) + \varepsilon_0$. In brief, the observed change (y) is the sum of the scaled responses to different forcings (X_i) and the noises which could not be explained by external forcings (ε_0). The sample errors (ε_{x_i}) result from the finite ensemble simulations. Here, an adaptation of the TLS-based optimal fingerprinting method referred to as regularized optimal fingerprinting is used. Details of the method can be found in Ribes et al. (2013) and Ribes and Terray (2013). The method is conducted for the area-averaged SAT over the TP and the 5-year non-overlapping means.

In the one-signal analysis, we regressed the vector of observation onto the simulated vector under individual external forcings (e.g., $y = \beta_{\mathrm{ALL}}\left(X_{\mathrm{ALL}} - \varepsilon_{x_{\mathrm{ALL}}}\right) + \varepsilon_0$). Considering the correlations between signals, the two-signal analysis (e.g., $y = \beta_{\mathrm{GHG}}\left(X_{\mathrm{GHG}} - \varepsilon_{x_{\mathrm{GHG}}}\right) + \beta_{\mathrm{AA}}\left(X_{\mathrm{AA}} - \varepsilon_{x_{\mathrm{AA}}}\right) + \varepsilon_0$) and three-signal analysis (e.g., $y = \beta_{\mathrm{GHG}}\left(X_{\mathrm{GHG}} - \varepsilon_{x_{\mathrm{GHG}}}\right) + \beta_{\mathrm{AA}}\left(X_{\mathrm{AA}} - \varepsilon_{x_{\mathrm{AA}}}\right) + \beta_{\mathrm{NAT}}\left(X_{\mathrm{NAT}} - \varepsilon_{x_{\mathrm{NAT}}}\right) + \varepsilon_0$) are also used to distinguish the influence of one forcing from the other or others. If the scaling factor β and the 90% confidence interval are significantly larger than 0, it indicates that the effect of a certain external forcing is detectable.

Following Jones et al. (2013) and X. Zhang et al. (2007), the warming trends induced by different external forcings can be estimated by multiplying the respective scaling factors. The attributable warming due to ALL forcing is estimated by multiplying the scaling factor from the one-signal analysis, and the attributable warming due to GHG, AA, or NAT forcing is estimated by multiplying the scaling factor from the three-signal analysis. The response to anthropogenic forcing (ANT) is inferred by subtracting the warming trend under NAT forcing from ALL forcing.

The attribution results can be used as an observational constraint to the future warming over the TP. Two methods are used in this study:

1. The observationally constrained projections are derived by multiplying the multi-model average of the SAT with the scaling factor of the ALL forcing from the one-signal analysis, viz. $\mathrm{SAT}_{\mathrm{SSP2-4.5}} \times \beta_{\mathrm{ALL}}$;
2. The observationally constrained projections are the sum of the SAT under GHG, AA, and NAT forcings, which are multiplied with the scaling factor of the GHG, AA, and NAT forcings from the three-signal analysis, respectively, viz. $\mathrm{SAT}_{\mathrm{SSP2-4.5-GHG}} \times \beta_{\mathrm{GHG}} + \mathrm{SAT}_{\mathrm{SSP2-4.5-aer}} \times \beta_{\mathrm{AA}} + \mathrm{SAT}_{\mathrm{SSP2-4.5-nat}} \times \beta_{\mathrm{NAT}}$.

3. Results

3.1. Observed TP Warming

Since 1961, a rapid warming trend is observed over the whole TP (Figure S2 in Supporting Information S1). This warming trend is significant ($p < 0.01$) in all SAT data sets, but the magnitudes vary among different observations, ranging from 0.21 to 0.33°C/decade for the area-averaged mean during the period of 1961–2020. Using more gauge records in comparison to other data sets (Wu & Gao, 2013; Y. Xu et al., 2009), CN05.1 has a warming rate which is the closest to the station observations (Figure S2e in Supporting Information S1) and hence we use this data set in the following analysis. According to CN05.1, the annual mean SAT has increased significantly over the TP during 1961–2020 with a trend of 0.33°C/decade ($p < 0.01$). The TP warmed by 1.95°C in the past six decades. It is almost two times of the global mean warming rate (1.04°C from 1960 to 2020) assessed by the Sixth Assessment Report of Intergovernmental Panel on Climate Change, and 1.3 times of the global land average (1.51°C from 1960 to 2020) (Gulev et al., 2021). The amplified warming over the TP is also significant in a shorter period during 1980–2020, when the warming magnitude for the TP (1.39°C) is 1.8 times of the global mean and 1.2 times of the global land average (Figure S2f in Supporting Information S1). We note that the BEST and CRU data sets, which are the most widely used gridded observations at global scale, have underestimated the observed warming trend over the TP by 18% and 36%, respectively, relative to CN05.1 (Figure S2e in Supporting Information S1).

The multi-model average of CMIP6 models under all external forcings well reproduces the observed TP warming (Figures S3 and S4 in Supporting Information S1). To quantify the relative contributions of individual external forcings on the TP warming, an optimal fingerprinting method together with the individual-forcing simulations are used, which had been widely used for detection and attribution analysis (Allen & Stott, 2003; Allen & Tett, 1999; Hasselmann, 1993; Hegerl & Zwiers, 2011). Regressing the observed SAT anomalies derived from CN05.1 onto the simulated SAT anomalies, the scaling factors β are significantly greater than zero and are consistent with unity for ALL and GHG forcing runs both for one- and two-signal analyses (Figures 1a and 1b). The responses to ALL and GHG forcings are detected in the observed warming trend over the TP, although the response is slightly underestimated by the models with β larger than 1, while the responses to AA and NAT forcings could not account for the observed TP warming. The increased concentrations of GHG could lead to the increase in net incoming longwave radiation flux at surface and further causes the rise of surface temperature (Figures S5d and S5f in Supporting Information S1). Reduced outgoing shortwave radiation flux related with snow/ice-albedo feedback under GHG forcing also contributes part of the warming trend (Figure S5c in Supporting Information S1). We further estimated the warming trends induced by different forcings by multiplying the respective scaling factors (see Section 2; Figure 1c; Table S3 in Supporting Information S1). For the observed TP warming during 1961–2020, a rate of 0.33 [0.23–0.43, 90% confidence interval] °C/decade is attributed to GHG forcing. The impacts of AA and NAT forcings are weak and negligible.

The detection and attributed results indicate that the observed warming trend in the past six decades is dominated by the GHG forcing. While the results are qualitatively consistent with a previous attribution on TP warming from 1961 to 2005 based on the earlier generation of climate models provided by CMIP5 (Zhou & Zhang, 2021), a weaker cooling trend under AA forcing is found during the longer period in this study (Table S3 in Supporting Information S1). Further analyses find this is related to a turning point of the SAT response to AA forcing, viz. from a cooling trend to a warming trend, since the late 2000s (Figure 2d). To tackle the air pollution problem, Eurasian countries has implemented a series of air pollution control measures in recent decades, which has effectively led to a dramatic decrease in anthropogenic aerosols and improved air quality (Ma et al., 2019; Y. Wang et al., 2015; Zheng et al., 2018). The reduced air pollution in Eurasia contributes to part of the TP warming trend after the late 2000s.

3.2. Future TP Warming

Under an anticipated worldwide clean air policy and continued emission of GHG, how will the TP SAT change in the future? *M4* are used to investigate the SAT responses to individual external forcings in the following analysis. We can obtain the similar attribution results from *M4* with that of the multi-model average of all 12 CMIP6 models, that is, the observed TP warming since 1961 is dominated by the GHG forcing with the scaling factors β and 90% confidence intervals larger than 0 for ALL and GHG forcing simulations (Figures 1 and 2).

Under SSP2-4.5 scenario, a continued warming trend over the TP is projected with a significant increasing rate of SAT at 0.31°C/decade ($p < 0.01$) during 2021–2100 derived from *M4* (Figure 2a; Figure S6a in Supporting

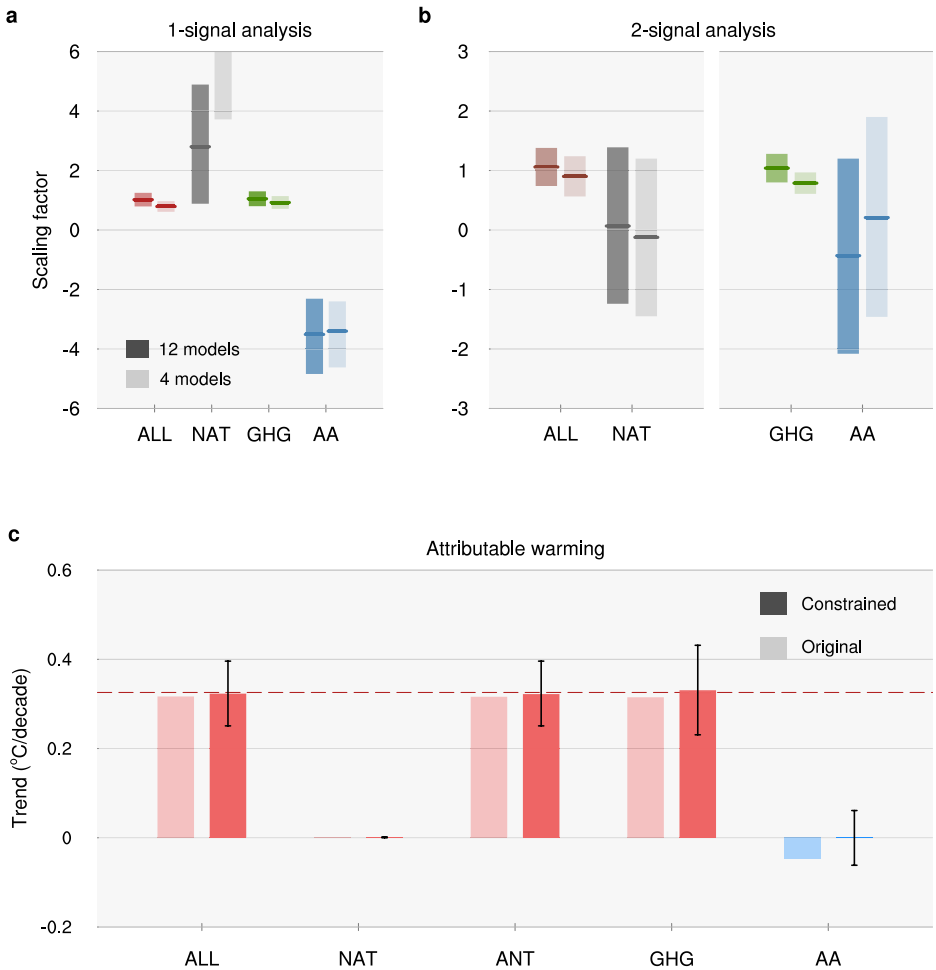

Figure 1. Detection and attribution analysis on the Tibetan Plateau warming during 1961–2020. (a) Scaling factors and the 90% confidence intervals of one-signal analysis for simulations under ALL, NAT, GHG, and AA forcings. (b) Scaling factors and the 90% confidence interval of two-signal analysis for ALL and NAT forcings, and for GHG and AA forcings. The results are derived from all models and *M4* (CanESM5, GISS-E2-1-G, MIROC6, and NorESM2-LM), respectively. (c) Attributable warming (°C/decade) due to ALL, NAT, ANT, GHG, and AA forcings derived from all models. For all contributions, the left hand side bars denote the original results, the right hand side bars and error bars denote the results constrained by the scaling factors and the 90% confidence intervals. The dotted line denotes the result for CN05.1.

Information S1). The warming trend is contributed by both the GHG and AA forcings (Figures S6c and S6d in Supporting Information S1). The increasing rates of TP SAT are 0.28 and 0.05°C/decade ($p < 0.01$) under GHG and AA forcings, respectively (Figures 2c and 2d). While the continued warming under GHG forcings during 2021–2100 is driven by both the net incoming shortwave and longwave radiation fluxes as in the past six decades (Figures S7a–S7f in Supporting Information S1), the increase in surface temperature under AA forcings is dominated by the net incoming shortwave radiation flux (Figures S7g and S7i in Supporting Information S1). The clean air quality policies and efficient enforcement assured by advanced technology and functioning institutions are expected to lead to a significant improvement of air quality at global scale (Rao et al., 2017). The decline of aerosols would cause significant increase in surface downwelling shortwave radiation flux through decreasing the reflection of shortwave solar radiation and the reduction of low-level clouds (Figures S7g and S7h in Supporting Information S1). Correspondingly, the reduced emission of anthropogenic aerosols will warm the TP in the following century as in the last decades (Figure 2d; Figure S6d in Supporting Information S1).

Previous studies generally constrained the future projections by multiplying the multi-model mean responses with the scaling factor of the ALL or ANT forcings, which assumes that the scaling factor based on historical observations and historical ALL or ANT forcing simulations also works in the same way in future projection and the

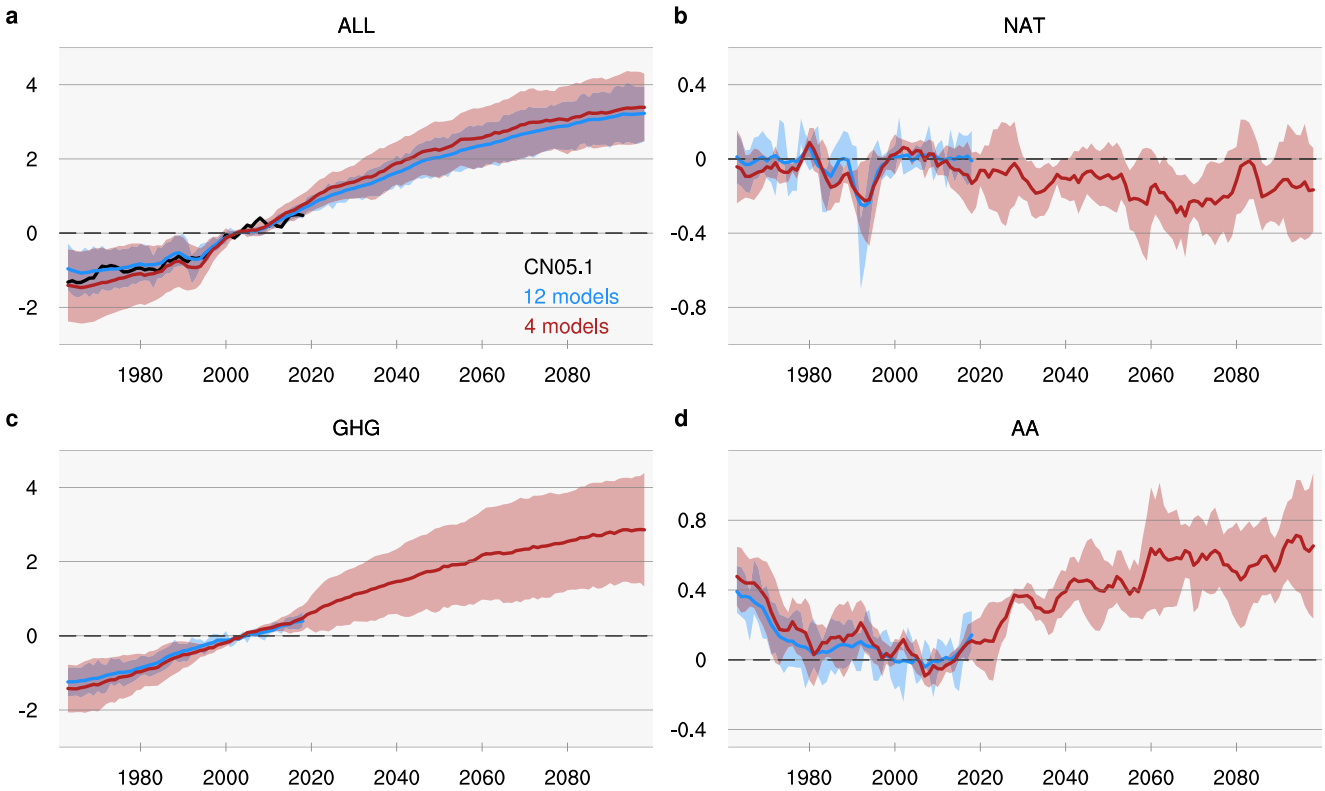

Figure 2. The evolution of annual mean surface air temperature (SAT) over the Tibetan Plateau (TP). Five year running mean annual mean SAT anomalies (°C) averaged over the TP relative to 1995–2014 derived from CN05.1 (black line) and the multi-model average under (a) all external forcings (ALL), (b) natural forcing alone (NAT), (c) greenhouse gases forcing alone (GHG), and (d) anthropogenic aerosol forcing alone (AA). The blue lines and shadings denote the results of all models, and the red lines and shadings denote the results of *M4*. The shading denotes the one standard deviation among the models.

impact of AA forcing is less important (Allen et al., 2000; Sun et al., 2014; Zhou & Zhang, 2021). Constrained by the scaling factor of the ALL forcing, the model spread of the simulated warming trend during 1961–2020 is reduced by nearly 90% (Figure S8a in Supporting Information S1). This method can effectively correct the overestimated or underestimated responses to all external forcings in the historical period. However, the model spread is even larger after adjustment in 2021–2100 under SSP2-4.5 scenario with an increased amplitude of 48% (Figure S8b in Supporting Information S1), indicating that this method is not suitable for the constraint of future projection.

Since the contributions of individual external forcings have changed, we need to constrain the responses to individual external forcings (GHG, AA, and NAT) rather than the response to the combined external forcings in future projection. To examine the above hypothesis, we perform a perfect model evaluation. We select one model except *M4* and treat its historical simulation (extended to 2020) as *pseudo-observation* and apply the attribution results of *M4* to predict the TP warming trend in 2021–2100 under SSP2-4.5 scenario. The projected TP warming trend derived from the selected model can be regarded as the "true" value. Based on *M4*, we find that the constrained projections according to GHG, AA, and NAT forcings separately are closer to the "true" values compared to those based on the scaling factors of ALL forcing for three quarters of the models (Figure 3). We also treat the ensemble mean of all models as the *pseudo-observation*. The constrained projection (0.32°C/decade) according to GHG, AA, and NAT forcings separately derived from *M4* is more comparable to the multi-model ensemble mean (0.32°C/decade), while the constrained projection (0.20°C/decade) according to ALL forcing greatly underestimates the future warming rate (Figure 3). The perfect model evaluation builds our confidence in the reliability of the new constraint method.

We further apply the attribution results for CN05.1 and individual external forcing simulations to constrain the future projections. Based on *M4*, under the SSP2-4.5 scenario, the TP would warm by 2.69°C in 2081–2100 relative to 1995–2014 under the best estimate of constraint by individual external forcings. Our constrained projection is 0.60°C cooler than the raw model output (Figure 4). For the near-term projection of 2041–2060, our constrained projection is 1.85°C, which is 0.44°C cooler than raw model output. We further estimate the

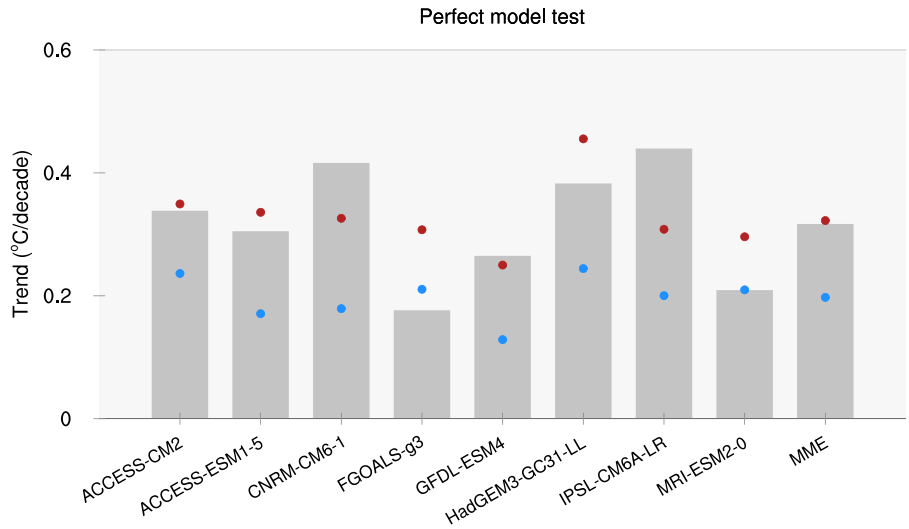

Figure 3. Perfect model evaluation. The linear trends in TP SAT (°C/decade) derived from individual models under SSP2-4.5 scenario during 2021–2100. Taking the historical simulations of individual models or the mean of all models (MME) as *pseudo-observations*, the blue dots denote the projections derived from *M4* constrained by the scaling factor of ALL forcing from 1-signal analysis, and the red dots denote the projections derived from *M4* constrained by the scaling factor of GHG, AA, and NAT forcings from 3-signal analysis.

contribution of individual external forcings constrained by the respective scaling factors. While the continued emission of GHG will warm the TP by 1.74 and 2.67°C in 2041–2060 and 2081–2100, respectively, the reduction of AA emission will also contribute to a warming of 0.10 and 0.13°C, respectively. The constrained contributions of both GHG and AA forcings to future warming over the TP are weaker that the raw results (Figure 4).

4. Conclusions

The TP has experienced a rapid warming since 1961 and the warming trend is projected to continue in the twenty-first century under different scenarios. Both the historical and future temperature changes are dominated

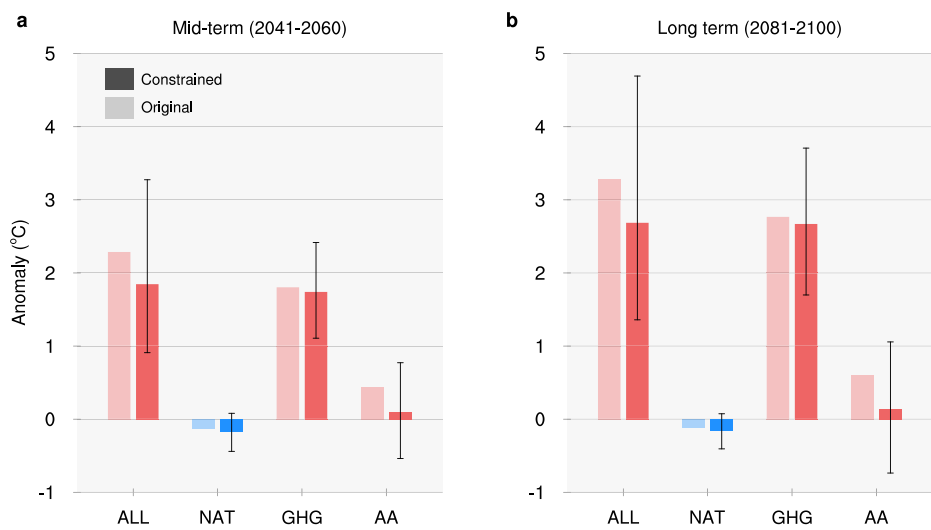

Figure 4. Assessed contributions of external forcings to future warming over the Tibetan Plateau (TP). The increase in surface air temperature (SAT) (°C) over the TP contributed by ALL, NAT, GHG, and AA forcings during (a) 2041–2060 and (b) 2081–2100 relative to 1995–2014. For ALL contributions, the left hand side bars denote the original results based on *M4*, the right hand side bars and error bars denote the results constrained by the respective scaling factors and the 90% confidence intervals from the 3-signal analysis. The increase in SAT attributed to ALL forcing is simultaneously constrained by the scaling factors of GHG, AA, and NAT forcings.

by anthropogenic forcings, including the GHG and aerosol forcings. While the GHG forcing has and will continue to warm the TP, the changes in AA forcing have partly offset the warming trend induced by GHG forcing before the late 2000s but will accelerate the warming rate induced by GHG forcing in the following century. The attribution results on historical changes can be used as an observational constraint for future projection. Since the composition of individual external forcings in the future differ to that in historical changes, we propose to constrain the responses to GHG, AA, and NAT forcings separately rather than to the combination of these forcings. Under SSP2-4.5 scenario, the projected TP warming at mid-century will warm by 1.85°C contributed by both GHG (1.74°C) and AA forcings (0.10°C).

Here we acknowledge that the turning point of the TP SAT response to AA forcing, that is, from a cooling trend to a warming trend, began around 2005 has and will continue to lead to a greater warming rate under all external forcings. The accelerated warming rate after 2005 is seen both in the externally forced response in observation (dashed line in Figure S3c of the Supporting Information S1), which is estimated as the component that evolves synchronously with the global mean sea surface temperature following Ting et al. (2011), and the historical simulations. Affected by strong internal climate variability, the trend over the short period of 2006–2020 in the direct observations is still weak (solid line in Figure S3c of the Supporting Information S1). Distinguishing and quantifying the relative contributions of internal modes and external forcings on the observed changes in TP SAT since 2005 deserve further study.

Our research focuses on the overall effects of anthropogenic aerosols. It should be noticed that the climate effects differ among different types of anthropogenic aerosols. While scattering aerosols (e.g., sulfates) induce cooling in the surface and lower atmosphere by reflecting incoming solar radiation back into space, light-absorbing aerosols (e.g., carbonaceous material) contribute to atmospheric heating by absorbing solar radiation (Szopa et al., 2021). The climate effects of different types of anthropogenic aerosols are not distinguished in DAMIP simulations but deserve further study. Besides anthropogenic aerosols, natural aerosols have also been found over the TP, which could further affect radiation balance at surface. In particular, dust is the most prominent type of aerosol on the TP, especially the northern slope (Jia et al., 2019; Y. Liu et al., 2015, 2022). Considering the response of dust to climate change (IPCC, 2013), further studies on the dust-climate feedbacks in future projections are needed.

To keep within 1.5 or 2°C of global warming proposed by the Paris Agreement, it is necessary to distinguish the contributions of greenhouses gas emissions and anthropogenic aerosol removal. Our new constraint method helps to estimate the future climate changes under the changed contributions of AA forcing and quantified the contributions of individual anthropogenic forcings. Since the removal of anthropogenic aerosol emission not only induces surface heating but also leads to changes in precipitation in the following decades (Peace et al., 2020; Samset, 2018; Samset et al., 2018; Wilcox et al., 2020), our results have broad implications for climate projections and are of great concern for climate change adaptation and mitigation activities.

Data Availability Statement

The CMIP6 model outputs are publicly available at the Earth System Grid Federation (https://esgf-node.llnl.gov/search/cmip6/). The models and simulations used in this study are listed in Table S2 of the Supporting Information S1. Anyone could download the corresponding data sets used in this study by selecting the corresponding models in Source ID, the corresponding simulations in Experiment ID, *mon* in Frequency, and *ts* in Variable. CRU is available at the CEDA Archive (https://catalogue.ceda.ac.uk/uuid/e0b4e1e56c1c4460b796073a31366980). BEST is available at Berkeley Earth data page (https://berkeleyearth.org/data/) by selecting Global Gridded Data, Global Monthly Land, Average Temperature (TAVG), and 1° × 1° Latitude-Longitude Grid in sequence. CN05.1 is provided by Climate Change Research Center, Chinese Academy of Sciences (https://ccrc.iap.ac.cn/resource/detail?id=228). The station observations used in Figures S1 and S2 of the Supporting Information S1 are provided by the China Meteorological Agency. Due to the data policy in China, the station observations are not publicly available via the website. Anyone could contact the China Meteorological Data Service Center (http://data.cma.cn/en) or the China Meteorological Administration (http://www.cma.gov.cn/en2014/aboutcma/contactus/) for detailed information on data acquisition. The data in this study is analyzed with NCAR Command Language (https://www.ncl.ucar.edu/Download/) and Scilab (https://www.scilab.org/). The core codes of the "optimal fingerprint" method are provided by Ribes et al. (2013) in http://www.umr-cnrm.fr/spip.php?article23&lang=en (rofpack_v1-0.zip).

Acknowledgments
This work is jointly supported by National Natural Science Foundation of China (Grant 41988101), the Strategic Priority Research Program of the Chinese Academy of Sciences (Grant XDA20060102), the Second Tibetan Plateau Scientific Expedition and Research (STEP) program (Grant 2019QZKK0102) and China Postdoctoral Science Foundation (Grants 2023T160631 and 2022M713093). We also acknowledge the support from Jiangsu Collaborative Innovation Center for Climate Change. Helpful discussions with Dr. Wenxia Zhang are appreciated.

References

Allen, M. R., & Stott, P. A. (2003). Estimating signal amplitudes in optimal fingerprinting, part I: Theory. *Climate Dynamics*, *21*(5–6), 477–491. https://doi.org/10.1007/s00382-003-0313-9

Allen, M. R., Stott, P. A., Mitchell, J. F. B., Schnur, R., & Delworth, T. L. (2000). Quantifying the uncertainty in forecasts of anthropogenic climate change. *Nature*, *407*(6804), 617–620. https://doi.org/10.1038/35036559

Allen, M. R., & Tett, S. F. B. (1999). Checking for model consistency in optimal fingerprinting. *Climate Dynamics*, *15*(6), 419–434. https://doi.org/10.1007/s003820050291

Azam, M. F., Wagon, P., Berthier, E., Vincent, C., Fujita, K., & Kargel, J. S. (2018). Review of the status and mass changes of Himalayan-Karakoram glaciers. *Journal of Glaciology*, *64*(243), 61–74. https://doi.org/10.1017/jog.2017.86

Bolch, T., Kulkarni, A., Kääb, A., Huggel, C., Paul, F., Cogley, J. G., et al. (2012). The state and fate of Himalayan glaciers. *Science*, *336*(6079), 310–314. https://doi.org/10.1126/science.1215828

Cao, L., Zhu, Y., Tang, G., Yuan, F., & Yan, Z. (2016). Climatic warming in China according to a homogenized data set from 2419 stations. *International Journal of Climatology*, *36*(13), 4384–4392. https://doi.org/10.1002/joc.4639

Chen, R., Li, H., Wang, X., Gou, X., Yang, M., & Wan, G. (2022). Surface air temperature changes over the Tibetan Plateau: Historical evaluation and future projection based on CMIP6 models. *Geoscience Frontiers*, *13*(6), 101452. https://doi.org/10.1016/j.gsf.2022.101452

Cuo, L., Zhang, Y., Wu, Y., & Hou, M. (2020). Desertification affecting the Tibetan Plateau between 1971–2015: Viewed from a climate perspective. *Land Degradation & Development*, *31*(15), 1956–1968. https://doi.org/10.1002/ldr.3575

Duan, A., & Xiao, Z. (2015). Does the climate warming hiatus exist over the Tibetan Plateau? *Scientific Reports*, *5*(1), 13711. https://doi.org/10.1038/srep13711

Gillett, N. P., Shiogama, H., Funke, B., Hegerl, G., Knutti, R., Matthes, K., et al. (2016). The detection and attribution model intercomparison project (DAMIP v1.0) contribution to CMIP6. *Geoscientific Model Development*, *9*(10), 3685–3697. https://doi.org/10.5194/gmd-9-3685-2016

Gulev, S. K., Thorne, P. W., Ahn, J., Dentener, F. J., Domingues, C. M., Gerland, S., et al. (2021). Changing state of the climate System. In V. Masson-Delmotte, P. Zhai, A. Pirani, S. L. Connors, C. Péan, S. Berger, et al. (Eds.), *Climate change 2021: The physical science basis. Contribution of working group I to the sixth assessment report of the intergovernmental panel on climate change* (pp. 287–422). Cambridge University Press. https://doi.org/10.1017/9781009157896.004

Harris, I., Jones, P. D., Osborn, T. J., & Lister, D. H. (2014). Updated high-resolution grids of monthly climatic observations—The CRU TS3.10 Dataset. *International Journal of Climatology*, *34*(3), 623–642. https://doi.org/10.1002/joc.3711

Hasselmann, K. (1993). Optimal fingerprints for the detection of time-dependent climate change. *Journal of Climate*, *6*(10), 1957–1971. https://doi.org/10.1175/1520-0442(1993)006<1957:OFFTDO>2.0.CO;2

Hegerl, G., & Zwiers, F. (2011). Use of models in detection and attribution of climate change. *WIREs Climate Change*, *2*(4), 570–591. https://doi.org/10.1002/wcc.121

Immerzeel, W. W., & Bierkens, M. F. P. (2012). Asia's water balance. *Nature Geoscience*, *5*(12), 841–842. https://doi.org/10.1038/ngeo1643

Immerzeel, W. W., van Beek, L. P. H., & Bierkens, M. F. P. (2010). Climate change will affect the Asian water towers. *Science*, *328*(5984), 1382–1385. https://doi.org/10.1126/science.1183188

IPCC. (2013). In T. F. Stocker, D. Qin, G.-K. Plattner, M. Tignor, S. K. Allen, J. Boschung, et al. (Eds.), *Climate change 2013: The physical science basis. Contribution of working group I to the fifth assessment report of the intergovernmental panel on climate change*. Cambridge University Press.

Jia, R., Luo, M., Liu, Y., Zhu, Q., Hua, S., Wu, C., & Shao, T. (2019). Anthropogenic aerosol pollution over the eastern slope of the Tibetan Plateau. *Advances in Atmospheric Sciences*, *36*(8), 847–862. https://doi.org/10.1007/s00376-019-8212-0

Jones, G. S., Stott, P. A., & Christidis, N. (2013). Attribution of observed historical near-surface temperature variations to anthropogenic and natural causes using CMIP5 simulations. *Journal of Geophysical Research: Atmospheres*, *118*(10), 4001–4024. https://doi.org/10.1002/jgrd.50239

Liang, Y., Gillett, N. P., & Monahan, A. H. (2020). Climate model projections of 21st century global warming constrained using the observed warming trend. *Geophysical Research Letters*, *47*(12), e2019GL086757. https://doi.org/10.1029/2019GL086757

Liu, X., Cheng, Z., Yan, L., & Yin, Z.-Y. (2009). Elevation dependency of recent and future minimum surface air temperature trends in the Tibetan Plateau and its surroundings. *Global and Planetary Change*, *68*(3), 164–174. https://doi.org/10.1016/j.gloplacha.2009.03.017

Liu, Y., Huang, J., Wang, T., Li, J., Yan, H., & He, Y. (2022). Aerosol-cloud interactions over the Tibetan Plateau: An overview. *Earth-Science Reviews*, *234*, 104216. https://doi.org/10.1016/j.earscirev.2022.104216

Liu, Y., Sato, Y., Jia, R., Xie, Y., Huang, J., & Nakajima, T. (2015). Modeling study on the transport of summer dust and anthropogenic aerosols over the Tibetan Plateau. *Atmospheric Chemistry and Physics*, *15*(21), 12581–12594. https://doi.org/10.5194/acp-15-12581-2015

Ma, Z., Liu, R., Liu, Y., & Bi, J. (2019). Effects of air pollution control policies on PM2.5 improvement in China from 2005 to 2017: A satellite-based perspective. *Atmospheric Chemistry and Physics*, *19*(10), 6861–6877. https://doi.org/10.5194/acp-19-6861-2019

O'Neill, B. C., Tebaldi, C., van Vuuren, D. P., Eyring, V., Friedlingstein, P., Hurtt, G., et al. (2016). The scenario model intercomparison project (ScenarioMIP) for CMIP6. *Geoscientific Model Development*, *9*(9), 3461–3482. https://doi.org/10.5194/gmd-9-3461-2016

Peace, A. H., Carslaw, K. S., Lee, L. A., Regayre, L. A., Booth, B. B. B., Johnson, J. S., & Bernie, D. (2020). Effect of aerosol radiative forcing uncertainty on projected exceedance year of a 1.5°C global temperature rise. *Environmental Research Letters*, *15*(9), 0940a6. https://doi.org/10.1088/1748-9326/aba20c

Peng, Y., Duan, A., Hu, W., Tang, B., Li, X., & Yang, X. (2022). Observational constraint on the future projection of temperature in winter over the Tibetan Plateau in CMIP6 models. *Environmental Research Letters*, *17*(3), 034023. https://doi.org/10.1088/1748-9326/ac541c

Rao, S., Klimont, Z., Smith, S. J., Van Dingenen, R., Dentener, F., Bouwman, L., et al. (2017). Future air pollution in the shared socio-economic pathways. *Global Environmental Change*, *42*, 346–358. https://doi.org/10.1016/j.gloenvcha.2016.05.012

Ribes, A., Planton, S., & Terray, L. (2013). Application of regularised optimal fingerprinting to attribution. Part I: Method, properties and idealised analysis. *Climate Dynamics*, *41*(11–12), 2817–2836. https://doi.org/10.1007/s00382-013-1735-7

Ribes, A., Qasmi, S., & Gillett, N. P. (2021). Making climate projections conditional on historical observations. *Science Advances*, *7*(4). https://doi.org/10.1126/sciadv.abc0671

Ribes, A., & Terray, L. (2013). Application of regularised optimal fingerprinting to attribution. Part II: Application to global near-surface temperature. *Climate Dynamics*, *41*(11–12), 2837–2853. https://doi.org/10.1007/s00382-013-1736-6

Rohde, R. A., & Hausfather, Z. (2020). The Berkeley Earth land/ocean temperature record. *Earth System Science Data*, *12*(4), 3469–3479. https://doi.org/10.5194/essd-12-3469-2020

Samset, B. H. (2018). How cleaner air changes the climate. *Science*, *360*(6385), 148–150. https://doi.org/10.1126/science.aat1723

Samset, B. H., Sand, M., Smith, C. J., Bauer, S. E., Forster, P. M., Fuglestvedt, J. S., et al. (2018). Climate impacts from a removal of anthropogenic aerosol emissions. *Geophysical Research Letters*, *45*(2), 1020–1029. https://doi.org/10.1002/2017GL076079

Shi, S., Li, J., Shi, J., Zhao, Y., & Huang, G. (2017). Three centuries of winter temperature change on the southeastern Tibetan Plateau and its relationship with the Atlantic Multidecadal Oscillation. *Climate Dynamics*, *49*(4), 1305–1319. https://doi.org/10.1007/s00382-016-3381-3

Stott, P. A., Mitchell, J. F. B., Allen, M. R., Delworth, T. L., Gregory, J. M., Meehl, G. A., & Santer, B. D. (2006). Observational constraints on past attributable warming and predictions of future global warming. *Journal of Climate*, *19*(13), 3055–3069. https://doi.org/10.1175/JCLI3802.1

Sun, Y., Zhang, X., Zwiers, F. W., Song, L., Wan, H., Hu, T., et al. (2014). Rapid increase in the risk of extreme summer heat in Eastern China. *Nature Climate Change*, *4*(12), 1082–1085. https://doi.org/10.1038/nclimate2410

Szopa, S., Naik, V., Adhikary, B., Artaxo, P., Berntsen, T., Collins, W. D., et al. (2021). Short-lived climate forcers. In V. Masson-Delmotte, P. Zhai, A. Pirani, S. L. Connors, C. Péan, S. Berger, et al. (Eds.), *Climate change 2021: The physical science basis. Contribution of working group I to the sixth assessment report of the intergovernmental panel on climate change* (pp. 817–922). Cambridge University Press. https://doi.org/10.1017/9781009157896.008

Ting, M., Kushnir, Y., Seager, R., & Li, C. (2011). Robust features of Atlantic multi-decadal variability and its climate impacts. *Geophysical Research Letters*, *38*(17), 1–6. https://doi.org/10.1029/2011GL048712

Tokarska, K. B., Stolpe, M. B., Sippel, S., Fischer, E. M., Smith, C. J., Lehner, F., & Knutti, R. (2020). Past warming trend constrains future warming in CMIP6 models. *Science Advances*, *6*, 9549–9567. https://doi.org/10.1126/sciadv.aaz9549

Wang, J., Yang, B., Ljungqvist, F. C., & Zhao, Y. (2013). The relationship between the Atlantic Multidecadal Oscillation and temperature variability in China during the last millennium. *Journal of Quaternary Science*, *28*(7), 653–658. https://doi.org/10.1002/jqs.2658

Wang, J., Yang, B., Qin, C., Kang, S., He, M., & Wang, Z. (2014). Tree-ring inferred annual mean temperature variations on the southeastern Tibetan Plateau during the last millennium and their relationships with the Atlantic Multidecadal Oscillation. *Climate Dynamics*, *43*(3–4), 627–640. https://doi.org/10.1007/s00382-013-1802-0

Wang, Y., Jiang, J. H., & Su, H. (2015). Atmospheric responses to the redistribution of anthropogenic aerosols. *Journal of Geophysical Research: Atmospheres*, *120*(18), 9625–9641. https://doi.org/10.1002/2015JD023665

Wang, Y., Yan, P., Ji, F., Huang, B., Fan, P., & Feng, G. (2023). Anthropogenic contribution to the rapid warming over the Tibetan Plateau. *Climate Dynamics*, *61*(1–2), 329–339. https://doi.org/10.1007/s00382-022-06576-8

Wilcox, L. J., Liu, Z., Samset, B. H., Hawkins, E., Lund, M. T., Nordling, K., et al. (2020). Accelerated increases in global and Asian summer monsoon precipitation from future aerosol reductions. *Atmospheric Chemistry and Physics*, *20*(20), 11955–11977. https://doi.org/10.5194/acp-20-11955-2020

Wu, J., & Gao, X. J. (2013). A gridded daily observation dataset over China region and comparison with the other datasets. *Chinese Journal of Geophysics*, *56*(4), 1102–1111. https://doi.org/10.6038/cjg20130406

Xu, X., Lu, C., Shi, X., & Gao, S. (2008). World water tower: An atmospheric perspective. *Geophysical Research Letters*, *35*(20), L20815. https://doi.org/10.1029/2008GL035867

Xu, Y., Gao, X., Shen, Y., Xu, C., Shi, Y., & Giorgi, F. (2009). A daily temperature dataset over China and its application in validating a RCM simulation. *Advances in Atmospheric Sciences*, *26*(4), 763–772. https://doi.org/10.1007/s00376-009-9029-z

Yang, M., Nelson, F. E., Shiklomanov, N. I., Guo, D., & Wan, G. (2010). Permafrost degradation and its environmental effects on the Tibetan Plateau: A review of recent research. *Earth-Science Reviews*, *103*(1–2), 31–44. https://doi.org/10.1016/j.earscirev.2010.07.002

Yang, X., Zhou, B., Xu, Y., & Han, Z. (2021). CMIP6 evaluation and projection of temperature and precipitation over China. *Advances in Atmospheric Sciences*, *38*(5), 817–830. https://doi.org/10.1007/s00376-021-0351-4

Yao, T., Bolch, T., Chen, D., Gao, J., Immerzeel, W., Piao, S., et al. (2022). *The imbalance of the Asian water tower*. Nature Reviews Earth & Environment. https://doi.org/10.1038/s43017-022-00299-4

Yao, T., Xue, Y., Chen, D., Chen, F., Thompson, L., Cui, P., et al. (2019). Recent third pole's rapid warming accompanies cryospheric melt and water cycle intensification and interactions between monsoon and environment: Multidisciplinary approach with observations, modeling, and analysis. *Bulletin of the American Meteorological Society*, *100*(3), 423–444. https://doi.org/10.1175/BAMS-D-17-0057.1

Yin, H., Li, M.-Y., & Huang, L. (2021). Summer mean temperature reconstruction based on tree-ring density over the past 440 years on the eastern Tibetan Plateau. *Quaternary International*, *571*, 81–88. https://doi.org/10.1016/j.quaint.2020.09.018

You, Q., Cai, Z., Pepin, N., Chen, D., Ahrens, B., Jiang, Z., et al. (2021a). Warming amplification over the Arctic Pole and Third Pole: Trends, mechanisms and consequences. *Earth-Science Reviews*, *217*, 103625. https://doi.org/10.1016/j.earscirev.2021.103625

You, Q., Cai, Z., Wu, F., Jiang, Z., Pepin, N., & Shen, S. S. P. (2021b). Temperature dataset of CMIP6 models over China: Evaluation, trend and uncertainty. *Climate Dynamics*, *57*(1–2), 17–35. https://doi.org/10.1007/s00382-021-05691-2

You, Q., Chen, D., Wu, F., Pepin, N., Cai, Z., Ahrens, B., et al. (2020). Elevation dependent warming over the Tibetan Plateau: Patterns, mechanisms and perspectives. *Earth-Science Reviews*, *210*, 103349. https://doi.org/10.1016/j.earscirev.2020.103349

Zhang, X., Zwiers, F. W., Hegerl, G. C., Lambert, F. H., Gillett, N. P., Solomon, S., et al. (2007). Detection of human influence on twentieth-century precipitation trends. *Nature*, *448*(7152), 461–465. https://doi.org/10.1038/nature06025

Zhang, Y., Li, J., Zheng, Z., & Zeng, S. (2021). A 479-year early summer temperature reconstruction based on tree-ring in the southeastern Tibetan plateau, China. *Atmosphere*, *12*(10), 1251. https://doi.org/10.3390/atmos12101251

Zheng, B., Tong, D., Li, M., Liu, F., Hong, C., Geng, G., et al. (2018). Trends in China's anthropogenic emissions since 2010 as the consequence of clean air actions. *Atmospheric Chemistry and Physics*, *18*(19), 14095–14111. https://doi.org/10.5194/acp-18-14095-2018

Zhou, T., & Zhang, W. (2021). Anthropogenic warming of Tibetan Plateau and constrained future projection. *Environmental Research Letters*, *16*(4), 044039. https://doi.org/10.1088/1748-9326/abede8

Zhu, Y.-Y., & Yang, S. (2020). Evaluation of CMIP6 for historical temperature and precipitation over the Tibetan Plateau and its comparison with CMIP5. *Advances in Climate Change Research*, *11*(3), 239–251. https://doi.org/10.1016/j.accre.2020.08.001